IEEE Photonics Journal
An IEEE Photonics Society Publication

Open Access

Coupled-Mode Theory of Multipath Interference in Quasi-Single Mode Fibers

Volume 7, Number 1, February 2015

M. Mlejnek
I. Roudas
J. D. Downie
N. Kaliteevskiy
K. Koreshkov

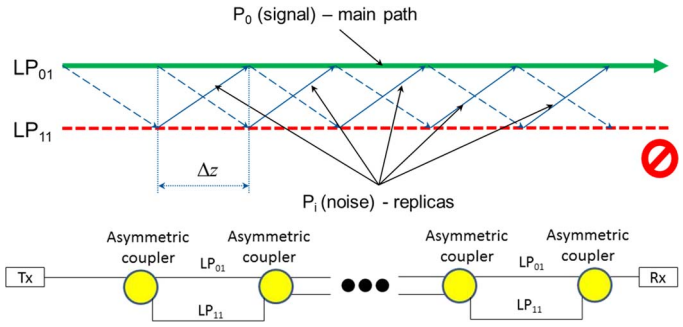

DOI: 10.1109/JPHOT.2014.2387260
1943-0655 © 2015 IEEE

IEEE photonics SOCIETY

IEEE

Coupled-Mode Theory of Multipath Interference in Quasi-Single Mode Fibers

M. Mlejnek, I. Roudas, J. D. Downie, N. Kaliteevskiy, and K. Koreshkov

Science and Technology Division, Corning Incorporated, Corning, NY 14831 USA
Corning Scientific Center, 194021 Saint Petersburg, Russia

DOI: 10.1109/JPHOT.2014.2387260

Manuscript received October 23, 2014; revised December 7, 2014; accepted December 10, 2014. Date of publication January 1, 2015; date of current version February 5, 2015. Corresponding author: M. Mlejnek (e-mail: mlejnekm@corning.com).

Abstract: We use the power coupled-mode theory to study the interplay between multipath interference (MPI) and differential mode attenuation (DMA) in quasi-single mode (QSM) fibers. The analytical expressions derived assuming two mode propagation in QSM fibers show that MPI scales differently as a function of the span length for low and high DMA. Furthermore, we derive analytical expressions for the performance improvement of long-haul coherent optical communication systems using QSM fibers, taking into account the impact of excess loss and MPI on system performance. From these expressions, we calculate the maximum allowable coupling coefficient for different values of the DMA. We show, for example, that a QSM fiber with an effective area of 250 μm^2, a coupling coefficient $\kappa \leq 6 \times 10^{-4}$ km^{-1}, and DMA equal to 4 dB/km offers a 1-dB performance advantage over a reference pure silica core single-mode fiber for spans of 100 km.

Index Terms: Quasi-single mode fiber, multipath interference, coherent optical communications, coupled-mode theory.

1. Introduction

Long-haul coherent optical communication systems currently operate close to the theoretical nonlinear capacity limit [1]. One way to boost optical fiber capacity beyond this limit is to further increase the effective area of the fiber in order to reduce nonlinear distortion [1]. An increase in effective area, while bringing the benefit of reducing nonlinear penalties, leads to enhanced sensitivity to micro-bend and macro-bend induced loss, and a somewhat related possibility of few spatial modes propagating in the fiber. In the former case, the designed fiber ends up having elevated loss that diminishes its reach. In the latter case, single mode transmission through a quasi-single mode (QSM) fiber, a few-mode fiber (FMF), or a multimode fiber (MMF) can suffer from multipath interference (MPI), which is a crosstalk effect that causes system performance degradation [2]–[10]. MPI can appear when the optical fiber supports, apart from the fundamental mode, at least one higher-order mode at the operating wavelength. Then, power coupling from the fundamental mode to the higher-order mode and back, at various random points during propagation, creates multiple delayed replicas of the signal that interfere with the signal at the receiver. This effect is similar in nature to the multipath crosstalk observed in the optical switch fabrics and add-drop multiplexers/demultiplexers of transparent optical networks. As in transparent optical networks, MPI leads to a rapid deterioration of the performance of a coherent optical communication system after the total power of the interferers exceeds a certain threshold.

Various physical mechanisms can lead to power coupling between modes and, eventually, MPI. We can roughly distinguish two MPI cases, discrete MPI, which can be generated locally at fiber splices and connectors and continuously-generated MPI along the fiber due to inter-modal coupling caused by index profile imperfections, twists and bends of the fiber on all spatial scales.

Initial studies on the topic of continuous MPI were performed in the context of the characterization of bimodal dispersion compensating fiber modules [2], [3]. More recent experiments [4]–[6] were conducted in order to quantify the impact of continuous MPI on the performance of coherent optical systems using single mode transmission over quasi-single mode, few-mode and multimode fibers. In addition, system-oriented theoretical models based on matrix multiplication describing field coupling between two mode groups at lumped points along transmission were proposed [7], [8]. Finally, the performance of adaptive electronic equalizers for continuous MPI compensation in coherent optical communication systems was studied in [9]–[11].

In the first part of this paper, in order to describe continuously-distributed MPI, we resort to power coupled-mode theory (CMT). More specifically, we consider a set of equations that describe the spatial evolution CW powers in two coupled modes co-propagating through the fiber at different speeds. The coupling between the modes is a result of random variations of the fiber index profile. Since we do not know exactly the realization(s) of the fiber index profile perturbations, we invoke the assumptions behind the derivation of the power CMT, as presented in [12]. We show that, despite its simplicity, the power CMT can provide useful insight into the MPI. Furthermore, we use the power CMT to study the effect of the differential modal attenuation (DMA) on MPI and summarize the work on the QSM fiber performance.

In the second part of this paper we derive analytical expressions for the performance improvement of a long-haul coherent optical system without in-line dispersion compensation based on QSM fiber, taking into account the impact of excess loss and MPI. In addition, we calculate the maximum allowable coupling coefficient for different values of the DMA. We show, for example, 1 dB performance advantage over a reference pure silica core single-mode fiber for 100 km spans of QSM fiber with an effective area of 250 μm^2, a coupling coefficient $\kappa \leq 6 \times 10^{-4}$ km^{-1}, and DMA equal to 4 dB/km.

The rest of the paper is organized as follows: In Section 2, we introduce the theoretical model for MPI and the performance improvement factor (PIF) that enables to quantify the impact of fiber MPI on the performance of a long-haul coherent optical system without in-line dispersion compensation. Section 3 focuses on the discussion of numerical results based on the theory of Section 2. The details of the calculation of the system performance degradation due to MPI are discussed in the Appendix.

2. Theoretical Model

2.1. Power CMT Model of MPI

There are several approaches to model fiber MPI caused by co-propagating modes. One such approach is based on i) the propagation of modal fields with field coupling occurring at prescribed, random or regular, points along the fiber, as schematically shown for two modes in Fig. 1 (top); and ii) MPI evaluation obtained by averaging the output signal over multiple realizations of the field couplings. In another approach, one i) performs averaging of the governing field propagation equations over the random realization of (continuously distributed) field coupling along the propagation distance first, arriving at power CMT [12] and then ii) solves the power CMT characterized by power coupling coefficients to evaluate the fiber MPI. The former approach is often used in simulations, since it allows simple treatment of effects caused by chromatic dispersion and nonlinearities. It will be briefly described in Section 2.2. To derive analytical results, we shall focus on the latter approach for the case of two CW modes next.

Consider the modal powers $P_\mu(z) \equiv \langle |A_\mu(z)|^2 \rangle$, $\mu = 0, 1$, given as an ensemble average of the modal field magnitude squared, $|A_\mu(z)|^2$, $\mu = 0, 1$. In the following, we will use the subscript 0 to

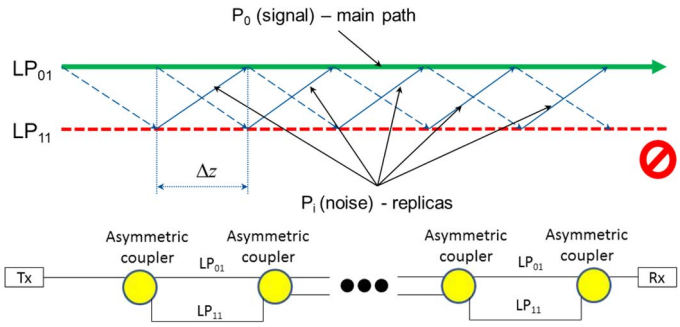

Fig. 1. (Top) Illustration of a 2-mode discrete coupling between the fundamental LP_{01} mode and the higher order mode LP_{11}. Δz denotes the length of a fiber segment, which is often referred to as waveplate, within which field propagation occurs without coupling. Coupling occurs in-between segments at their connections. The LP_{11} mode is not detected. (Bottom) Two-mode optical fiber can be represented as a series of cascaded asymmetric Mach-Zehnder interferometers.

denote quantities referring to the fundamental mode and the subscript 1 to denote quantities referring to the higher order mode. The evolution of the modal powers is described by the equations

$$\begin{aligned} dP_0/dz &= -\alpha_0 P_0 + \kappa(P_1 - P_0) \\ dP_1/dz &= -\alpha_1 P_1 + \kappa(P_0 - P_1). \end{aligned} \tag{1}$$

In (1), the explicit spatial dependence was omitted for brevity. On the right hand side of (1), we have terms describing the modal loss, different for the two modes, using the attenuation coefficients α_0 and α_1. The difference in the values of these attenuation coefficients constitutes the DMA, a focal point of our study. The coupling of the two modes is described by the terms that involve the average power coupling coefficient κ (assumed positive). This average coupling coefficient contains the effects of refractive index perturbation along the propagation distance z, through its power spectrum, and depends on the difference of the phase velocities of the modes [12]. The coupling coefficient also depends on the transverse spatial profile of the modal fields, invoking the selection rules between the modes that can couple or are forbidden to couple.

Assuming that only the fundamental mode is launched into the fiber, the initial conditions are $P_0(0) = 1$ and $P_1(0) = 0$. Then, the solution of (1) is

$$\begin{aligned} P_0(z) &= \frac{1}{\delta}\left[\delta \cosh\left(\frac{\delta z}{2}\right) + \Delta\alpha \sinh\left(\frac{\delta z}{2}\right)\right] e^{-(\kappa+\alpha)z} \\ P_1(z) &= \frac{2\kappa}{\delta}\sinh\left(\frac{\delta z}{2}\right) e^{-(\kappa+\alpha)z} \end{aligned} \tag{2}$$

where we defined the DMA as $\Delta\alpha \equiv \alpha_1 - \alpha_0$, introduced the average attenuation coefficient $\alpha \equiv (\alpha_1 + \alpha_0)/2$, and used the shorthand notation $\delta \equiv \sqrt{\Delta\alpha^2 + 4\kappa^2}$.

In the discrete case [3], MPI is defined by $MPI \equiv \sum_i P_i/P_s$, where the sum runs over all possible interference paths, P_i denoting the ith delayed signal power replica, and P_s denoting the average power of the signal incident on the receiver. In the case of continuous MPI, modeled by (1), we use a different, but equivalent expression to calculate MPI: $MPI = (P_{out} - P_{signal})/P_{signal}$, with P_{out} denoting the total power in the fundamental mode, at the end of the span length L, and P_{signal} denoting the power in the fundamental mode, assuming no back-coupled power from the higher-order mode, i.e., $P_{signal} = \exp[-(\kappa + \alpha_0)L]$, as shown below.

Examining the extreme case when power coupling from the higher-order mode back to the fundamental mode is negligible, the first of the equations (1) becomes

$$dP_0/dz = -(\alpha_0 + \kappa)P_0 \tag{3}$$

with solution

$$P_{\text{signal}} \equiv P_0(L) = P_0(0)\exp[-(\alpha_0 + \kappa)L]. \tag{4}$$

We observe that the power coupling coefficient is directly added to the attenuation coefficient of the fundamental mode, since the power coupled from the fundamental mode to the higher order mode is lost.

It is also instrumental to compare P_{out} with the power of a single-mode fiber with the same attenuation as the fundamental mode above, α_0. We can define the excess loss of the QSM fiber over the loss of a single-mode fiber as $EL \equiv P_{\text{out}}/[P_0(0)\text{e}^{-\alpha_0 L}]$ and study its dependence on various parameters and its influence on the fiber performance. Excess loss represents an added term to the fiber loss that is due to mode coupling and cannot be compensated at the receiver. Hence, the relevant limit for fiber long-haul transmission is the limit of weak coupling. For example, in the limit $\Delta\alpha^2 \gg 4\kappa^2$, i.e., in the DMA-dominant regime, $EL \approx P_{\text{signal}}/[P_0(0)\text{e}^{-\alpha_0 L}] = \exp[-\kappa L]$.

We interpret the 0-th mode as the LP_{01} mode of a fiber and the 1-st mode as the LP_{11} mode. Using the solution (2), we arrive at the following expression for the MPI parameter:

$$MPI = \left[\cosh\left(\frac{\delta L}{2}\right) + \frac{\Delta\alpha}{\delta}\sinh\left(\frac{\delta L}{2}\right)\right] e^{-\Delta\alpha\cdot L/2} - 1. \tag{5}$$

We are interested in the weak coupling regime $\kappa L \ll 1$ in two-mode fibers. In this limit, (5) leads to the simplified expression

$$MPI = \frac{\Delta\alpha L - 1 - e^{-\Delta\alpha L}}{\Delta\alpha^2}\kappa^2 + O(\kappa^3). \tag{6}$$

This expression has several interesting limits: I) When $\kappa = 0$, i.e., in the case of no coupling, we obtain $MPI = 0$, as expected, independent of the value of DMA; II) in the absence of DMA, i.e., when $\Delta\alpha = 0$, we obtain $MPI_0 = (\kappa L)^2/2$, where the subscript 0 denotes zero DMA; III) in the case of high DMA, i.e., when $\Delta\alpha^2 \gg 4\kappa^2$, we arrive at $MPI_{\text{DMA}} = \kappa^2 L/\Delta\alpha$. From these results, it transpires that the MPI can be reduced if we allow for substantial DMA, $MPI_{\text{DMA}} < MPI_0$, since

$$MPI_{\text{DMA}} = \frac{\kappa^2 L}{\Delta\alpha} = \frac{2}{\Delta\alpha L}\frac{(\kappa L)^2}{2} = \frac{2}{\Delta\alpha L} \times MPI_0. \tag{7}$$

We observe that MPI_{DMA} is smaller than MPI_0, if $\Delta\alpha L > 1$. The above expressions also lead to an interesting observation about the propagation length dependence of the MPI: It is quadratic in the case of small DMA, while linear in the presence of substantial DMA. This is shown in Fig. 2.

Continuous MPI is often simulated as a limit of a number of discrete multi-mode fiber segments, where power coupling occurs at the connections between fiber segments (see Fig. 1). To formulate such a discrete power coupling model, we cut the fiber into M segments of length Δz. Then, the power attenuation matrix can be written as

$$D_p = e^{-\alpha\Delta z}\begin{pmatrix} e^{\Delta\alpha\Delta z/2} & 0 \\ 0 & e^{-\Delta\alpha\Delta z/2} \end{pmatrix} \tag{8}$$

and the power coupling matrix as

$$C_p = \begin{pmatrix} 1-\varepsilon & \varepsilon \\ \varepsilon & 1-\varepsilon \end{pmatrix}, \quad \varepsilon \equiv \kappa\Delta z. \tag{9}$$

The channel power transfer matrix is then given by

$$T_p = C_p \prod_{j=1}^{M} D_p C_p. \tag{10}$$

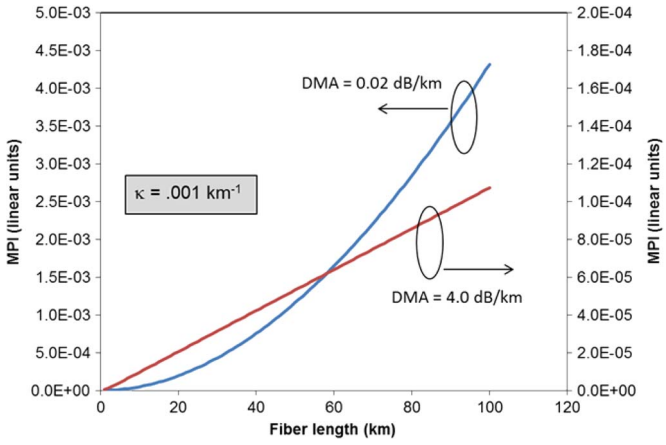

Fig. 2. MPI (in linear units) dependence on the propagation length. The dependence is quadratic when the DMA satisfies $\Delta\alpha^2 \ll 4\kappa^2$, while linear when $\Delta\alpha^2 \gg 4\kappa^2$. LP_{01} attenuation of 0.16 dB/km and $\kappa = 0.001$ km^{-1} were assumed.

The matrix T_p connects the input powers to the output powers:

$$P_{out} = T_p P_{in}, \quad P_{in} = (1 \quad 0)^T, \quad P_{out} = (P_0 \quad P_1)^T. \tag{11}$$

This model also allows one to generalize the power CMT equations (1) to account for possible inhomogeneities of modal loss and coupling along the fiber. Relations (8)–(11) can be used to study the convergence of the discrete model results to the continuous analytical solution.

2.2. Discrete Field Coupling Model of MPI

Fig. 1 (bottom) shows a simplified representation of an optical fiber supporting the LP_{01} and LP_{11} mode groups. In this schematic, we assume that the modes inside each mode group are fully degenerate and, therefore, we can assume that each mode group behaves as one mode. As in the previous section, we assume that the light is injected in the fundamental mode exclusively. At various random locations along the fiber, which are denoted by yellow circles, light couples from one mode to another. Therefore, the optical fiber is equivalent to a series of cascaded asymmetric Mach-Zehnder interferometers. As above, we ignore chromatic dispersion and nonlinearities in our model.

To formulate the discrete MPI model in terms of propagating fields, we cut again the fiber into M segments of length Δz. The field attenuation matrix in a fiber segment can then be written as

$$D_{f,j} = e^{-\alpha_j \Delta z/2} \begin{pmatrix} e^{\Delta\alpha_j \Delta z/4} & 0 \\ 0 & e^{-\Delta\alpha_j \Delta z/4} \end{pmatrix}. \tag{12}$$

One possible form of the fields coupling matrix can be

$$C_{f,j} = \begin{pmatrix} \cos\varphi_j & i\sin\varphi_j \\ i\sin\varphi_j & \cos\varphi_j \end{pmatrix} \tag{13}$$

with $\sin^2\varphi_j \equiv \varepsilon_j = \kappa(z_j)\Delta z, \ 1 \le j \le M+1$.

The channel field transfer matrix is then expressed as

$$T_f = C_{M+1} \prod_{j=1}^{M} D_{f,j} C_{f,j} \tag{14}$$

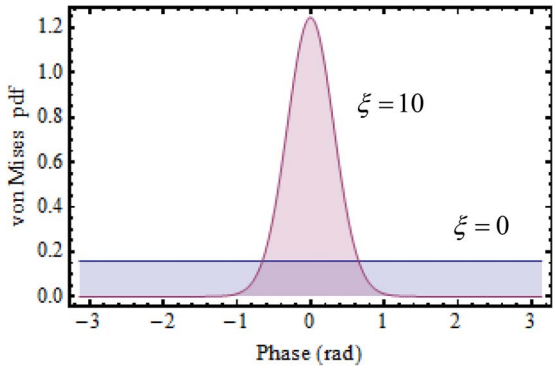

Fig. 3. Von-Mises distribution with a zero mean.

and the output fields are calculated using

$$A_{out} = T_f A_{in},\ A_{in} = (1 \quad 0)^T,\ A_{out} = (A_0 \quad A_1)^T. \tag{15}$$

Assuming a homogeneous fiber, i.e., with identical average loss and DMA in all the segments, $\alpha_j = \alpha,\ \Delta\alpha_j = \Delta\alpha\ \forall j$, the useful signal in the fundamental mode is given by

$$A_s = e^{-M\alpha\Delta z/2} e^{M\Delta\alpha\Delta z/4} \prod_{j=1}^{M+1} \cos\varphi_j \tag{16}$$

and we used $MPI' \equiv |A_0 - A_s|^2/A_s^2$ as a definition of MPI parameter for the field coupling model.

The individual realizations of the field coupling along the fiber are determined by the random parameters $\varphi_j,\ 1 \le j \le M+1$, which are be drawn from an appropriate distribution. Strong coupling, relevant, e.g., for polarization mode dispersion description, is characterized by a uniform distribution of φ's in the interval $(-\pi, \pi)$. To capture the weak coupling limit of interest here, we use arbitrarily the von-Mises distribution (with zero mean) that allows us to model a more localized distribution of φ's

$$p_\varphi(\varphi;\xi) = \frac{e^{\xi\cos\varphi}}{2\pi I_0(\xi)}, \quad -\pi \le \varphi \le \pi \tag{17}$$

where the parameter ξ^{-1} is related to the spread of the principal axes of the coupler (13) on the equator of the Poincaré sphere and $I_0(\xi)$ is the zeroth-order modified Bessel function of the first kind. Setting $\xi = 0$ leads to a uniform distribution, while larger values of ξ lead to Gaussian-like distributions caused by an approximate alignment of the principal axes of the couplers (see Fig. 3). Zero mean aligns the principal axes of the coupler (13) around the x-axis of the Poincaré sphere.

2.3. Calculation of the Performance Improvement Factor (PIF)

To quantify the difference between two coherent optical systems using two different optical fibers, we compare the optimal Q-factor for the fiber under study, Q_0, and the optimal Q-factor of a reference fiber, $Q_{0,r}$. We define the performance improvement factor (PIF), in linear scale, as $F \equiv (Q_0/Q_{0,r})^2$ and, in logarithmic scale, as $F[\text{dB}] \equiv 10\log F$.

2.3.1. PIF for Transmission Over an Ideal Single-Mode Fiber

The Q-factor of a coherent optical system using an ideal single-mode fiber and no in-line chromatic dispersion compensation can be well described by the analytical asymptotic

relationship [13]–[15]

$$Q^2 = A\frac{P}{\widetilde{\alpha}_i + \widetilde{\gamma}_i P^3} \tag{18}$$

where A is a multiplicative coefficient depending on the modulation format and the receiver filter, P is the total average launch power per channel (in both polarizations), $\widetilde{\alpha}_{\rm i}$ is the amplified spontaneous emission (ASE) noise variance, and $\widetilde{\gamma}_{\rm i}P^3$ is the nonlinear noise variance. The index i in the coefficients $\widetilde{\alpha}_{\rm i}$, $\widetilde{\gamma}_{\rm i}$ denotes an "ideal" single-mode fiber (i.e., without a higher-order mode present). Notice than in (18) and henceforth, P corresponds to P_0 that was used in Section 2.1.

The ideal single-mode fiber is assumed to have an effective area $A_{\rm eff}$, a nonlinear index coefficient n_2, and an attenuation coefficient α_0. Each optical fiber span is followed by an optical amplifier of gain equal to the span loss $G = \exp(\alpha_0 L)$ and noise figure $F_{\rm A}$. In this case, the coefficients $\widetilde{\alpha}_{\rm i}$, $\widetilde{\gamma}_{\rm i}$ for the center WDM channel of carrier wavelength λ depend on the system parameters as follows:

$$\widetilde{\alpha}_i \approx hf_0 N_s F_A \Delta\nu e^{\alpha_0 L} \tag{19}$$

$$\widetilde{\gamma}_i \approx \left(\frac{2}{3}\right)^3 \gamma^2 N_s \frac{\ln\left(\pi^2|\beta_2|N_{ch}^2 R_s^2/\alpha_0\right)}{\pi|\beta_2|R_s^3\alpha_0}\Delta\nu \tag{20}$$

where h is Planck's constant, f_0 is the center WDM channel carrier frequency $(f_0 = c/\lambda)$, $N_{\rm s}$ is the number of spans, L is the span length, $\Delta\nu$ is the resolution bandwidth for the measurement of the ASE noise from the optical amplifiers, $\gamma = 2\pi n_2/(\lambda A_{\rm eff})$ is the nonlinear coefficient of the fiber, β_2 is the group velocity dispersion (GVD) parameter, $N_{\rm ch}$ is the number of WDM channels, and $R_{\rm s}$ is the symbol rate. The speed of light in vacuum is denoted as c.

At the optimum operating point, the Q-factor takes its maximal value

$$Q_{0i}^2 = A\left(\frac{4}{27\widetilde{\alpha}_i^2\widetilde{\gamma}_i}\right)^{1/3}. \tag{21}$$

First, we compare two systems with the same exact system parameters using ideal single-mode fibers with different effective areas and attenuation coefficients. In this case, the PIF, in linear scale, is given by

$$F_i = \frac{Q_{0i}^2}{Q_{0,r}^2} \approx \left[\frac{A_{eff}^2}{A_{eff,r}^2}\frac{\alpha_0}{\alpha_{0,r}}e^{2(\alpha_{0,r}-\alpha_0)L}\right]^{1/3}. \tag{22}$$

2.3.2. PIF for Transmission Over QSM Fiber

The PIF, in the extreme case when there is no MPI at the output of the receiver, e.g., due to perfect electronic MPI compensation, can be given by modifying (22) to include the impact of the excess loss

$$F_c = \frac{Q_0^2}{Q_{0,r}^2} \approx \left[\frac{A_{eff}^2}{A_{eff,r}^2}\frac{\alpha_0+\kappa}{\alpha_{0,r}}e^{2(\alpha_{0,r}-\alpha_0-\kappa)L}\right]^{1/3} \tag{23}$$

where

$$Q_0^2 = A\left(\frac{4}{27\widetilde{\alpha}^2\widetilde{\gamma}}\right)^{1/3} \tag{24}$$

$$\widetilde{\alpha} \approx hf_0 N_s F_A \Delta\nu e^{(\alpha_0+\kappa)L} \tag{25}$$

$$\widetilde{\gamma} \cong \left(\frac{2}{3}\right)^3 \gamma^2 N_s \frac{\ln\left[\pi^2|\beta_2|N_{ch}^2 R_s^2/(\alpha_0+\kappa)\right]}{\pi|\beta_2|R_s^3(\alpha_0+\kappa)}\Delta\nu. \tag{26}$$

In (23), we assumed that the reference fiber is again an ideal single-mode fiber. Note that we used the symbol F_c (for compensated systems) to differentiate from the case of the ideal single-mode fiber, which is denoted by F_i. In addition note that we dropped the index i in the coefficients $\widetilde{\alpha}, \widetilde{\gamma}$ to indicate that the latter quantities are now affected by the excess loss of the QSM fiber.

Next, we examine the opposite extreme case when there is MPI at the output of the receiver and there is no electronic MPI compensation. We assume that the MPI acts as an equivalent Gaussian noise added to the ASE and nonlinear noise during signal propagation. Then, the Q-factor of a coherent optical system using QSM fiber can be described by the analytical relationship

$$Q^2 = A\frac{P}{\widetilde{\alpha} + \widetilde{\beta}P + \widetilde{\gamma}P^3} \tag{27}$$

where $\widetilde{\beta}P$ is the MPI noise variance at the input of the coherent optical receiver. It is shown in the Appendix that $\widetilde{\beta} = N_s\Delta\nu\, MPI/R_s$.

The presence of MPI noise changes the Q-factor at the optimum operating point to

$$Q_{\max}^2 = \frac{Q_0^2}{1 + \widetilde{\beta}Q_0^2/A}. \tag{28}$$

By repeating the calculation of the PIF using (24)–(28), we obtain for the "uncompensated" PIF

$$F_u = \frac{Q_{\max}^2}{Q_{0,r}^2} = \frac{F_c}{1 + C_r F_c \cdot MPI} \tag{29}$$

where F_c is given by (23), and C_r is a multiplicative coefficient, depending on the parameters of the reference system exclusively

$$C_r = \left[\frac{\pi|\beta_{2r}|\alpha_{0,r}}{2(hf_0F_A)^2 e^{2\alpha_{0,r}L}\gamma_r^2 \ln\left(\pi^2|\beta_{2r}|N_{ch}^2R_s^2/\alpha_{0,r}\right)}\right]^{1/3} \tag{30}$$

with γ_r given by $\gamma_r = 2\pi n_{2,r}/(\lambda A_{\text{eff},r})$.

3. Results and Discussion

3.1. Analytical MPI Model

In Fig. 4, we show contour plots that allow the determination of minimal DMA, or the minimal loss of the 1-st mode assuming the 0-th mode loss is known, for a given maximal allowed MPI and power coupling coefficient in the regime III) defined in Section 2.1. It was shown in [17], using an MPI emulator, that MPI needs to be smaller than approximately -26 dB for the MPI penalty to be smaller than 1 dB for a 256 Gb/s PM-16QAM signal at BER values of 10^{-3}. Fig. 5 illustrates the allowable minimal 1-st mode attenuation coefficient dependence on the coupling constant, given a specified level of MPI and assuming 80 km span length and typical zeroth mode attenuation.

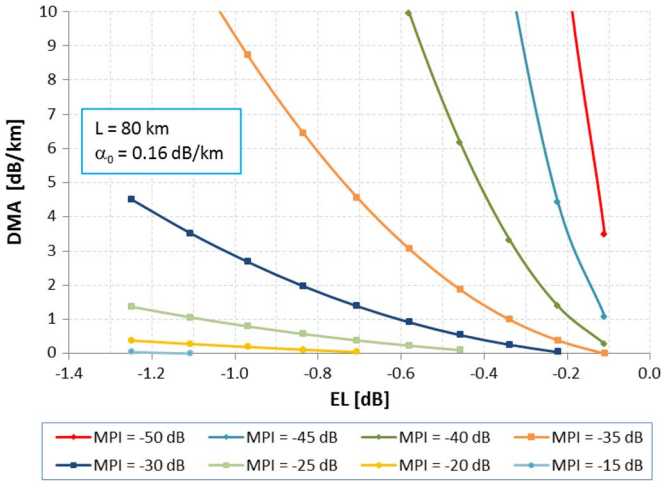

Fig. 4. Minimal LP_{11} mode attenuation that is needed for various coupling coefficients and allowed MPI. 80 km propagation length is assumed.

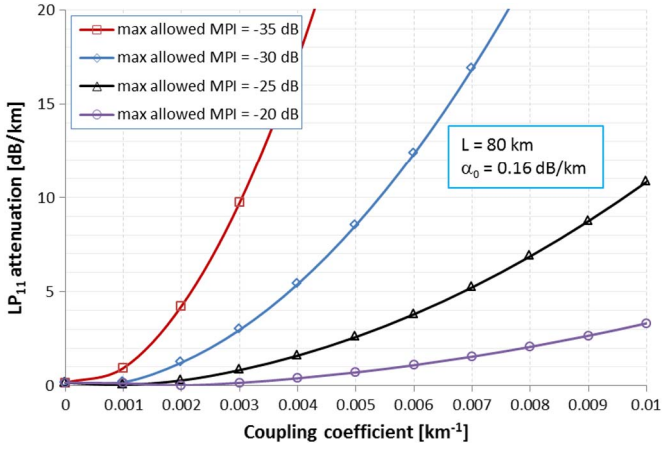

Fig. 5. Minimal LP_{11} mode attenuation needed for MPI to be lower than a prescribed value for a 80 km propagation length and 0.16 dB/km LP_{01} attenuation.

Using the continuous power coupling model of Section 2.1, we can study the interplay of allowable fiber MPI, excess loss, DMA, coupling κ, and propagation distance L. For example, given a maximum required EL, Fig. 6 can be used to determine the maximum allowable MPI level for a fiber with known DMA and L. From these values of excess loss, DMA, and L, κ can be determined if desired. This may be a practical alternative way to estimate fiber's coupling coefficient.

3.2. Discrete MPI Modeling

In practice, as mentioned above, the continuous MPI is often simulated as a limit of a number of discrete multi-mode fiber segments, where power coupling occurs at the connections between adjacent fiber segments (see Fig. 1). While such calculations using power CMT yield the same qualitative behavior as described by (6) and its various limits, such as quadratic and linear dependence of MPI on the propagation length, Fig. 7 shows that, e.g., more than 1000 segments may be necessary to produce the right quantitative answer in the regime III) discussed in Section 2.1. Note the qualitative difference in the convergence dependence on DMA in Fig. 7.

Nevertheless, discrete power and field coupling models can be used to study the statistics of MPI using Monte Carlo methods. Next, we study the discrete field coupling model described in

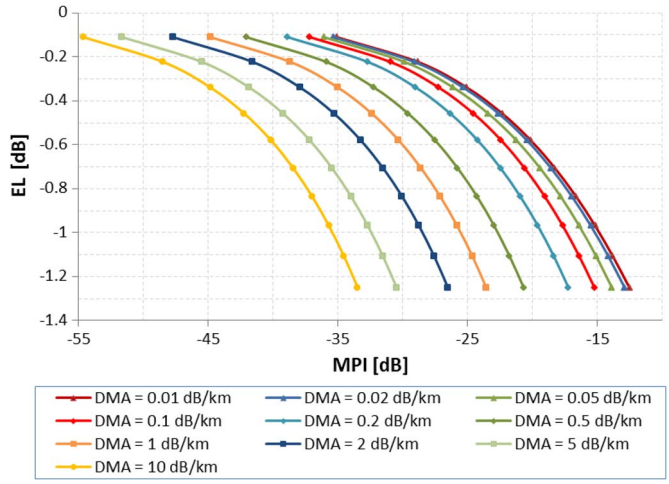

Fig. 6. Excess loss dependence on MPI and DMA for $\alpha = 0.16$ dB/km^{-1} and $L = 80$ km.

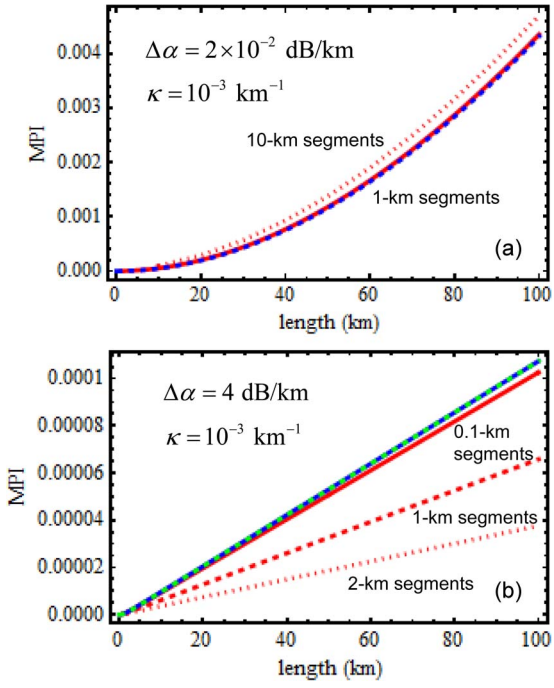

Fig. 7. MPI dependence on the propagation length. (a) Low DMA case. Blue dashed line: continuous *MPI* solution (6). Red-dot line: 10 km segments used. Red-dashed line: 1 km segments used. (b) High DMA case. Blue dashed line: continuous *MPI* solution (6). Cyan line: approximation $MPI_{DMA} = \kappa^2 L/|\Delta\alpha|$ in (7). Red lines: discrete power coupling model with different segments lengths.

Section 2.2., in conjunction with field CMT. The weak two-mode field coupling is mimicked using the unitary coupling matrices (13) with principal axes distributed along a portion of the equator of the Poincaré sphere following (17). The parameter ξ in (17) is chosen such that the mean of the power splitting ratio is equal to the nominal value of the power coupling parameter $\varepsilon \equiv \kappa\Delta z$, i.e.,

$$\varepsilon = \int_{-\pi}^{\pi} d\varphi \sin^2\varphi p_\varphi(\varphi;\xi) = \frac{I_1(\xi)}{\xi I_0(\xi)}. \tag{31}$$

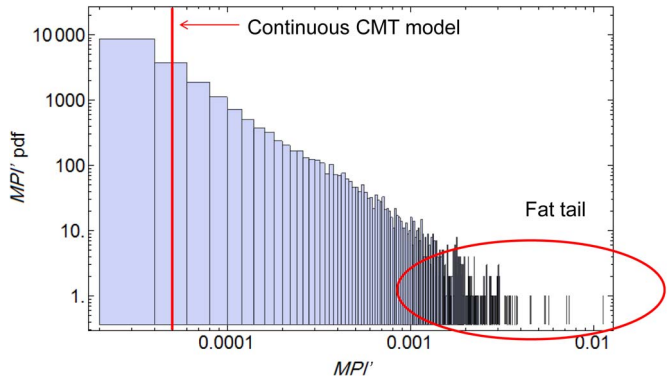

Fig. 8. Discrete field CMT model: The mean MPI parameter *MPI'* predicted by the discrete field CMT model is approximately the same as the one predicted by the continuous power CMT analytical model (1) and is equal to –43 dB (black line) but the actual *MPI'* takes values in a large range.

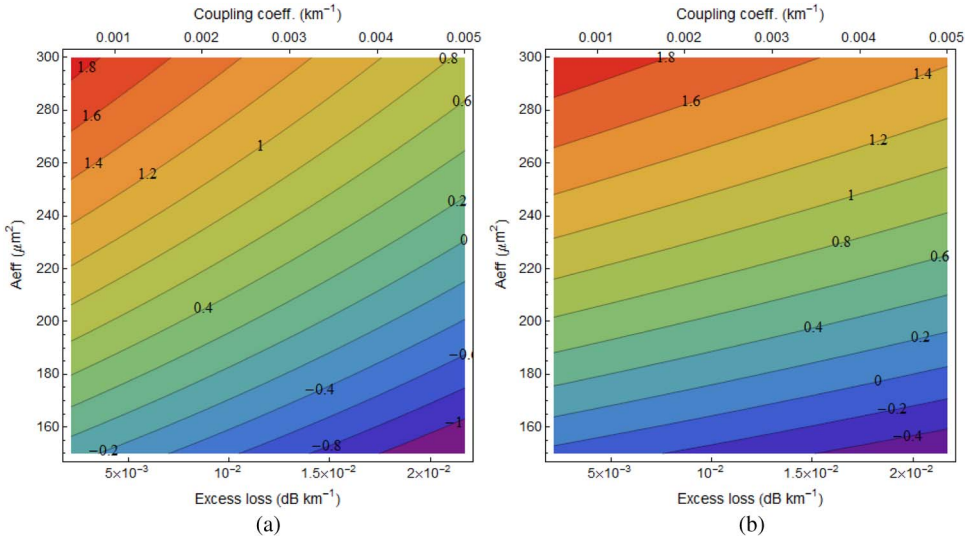

Fig. 9. PIF contours (in dB) as a function of the excess loss or the coupling coefficient and the effective area for a coherent optical communications system with perfect electronic MPI compensation at the receiver. (a) 100 km spans. (b) 50 km spans.

For instance, for $\varepsilon \equiv \kappa \Delta z = 10^{-3}$, we obtain $\xi = 999.5$; therefore, φ follows a narrow Gaussian-like probability distribution function that resembles a Dirac δ-distribution.

The MPI distribution for 10 000 realizations of a 10 km fiber span using 10 $\times$ 1 km fiber segments is shown in Fig. 8. The mean of the histogram agrees well with the prediction of the continuous power CMT model (6). However, the actual MPI takes values in a large range. Even though the calculation is performed for a finite number of interfering fields, the MPI histogram implies a slow polynomial decay of the right tail of the distribution (i.e., "fat-tailed distribution"). Since the variance of random variables described by pdf with fat tails can be unbounded, the central limit theorem might not apply. Consequently, a fat-tailed MPI distribution might result for multiple spans as well. This can have an important implication for the system outages.

3.3. PIF

To investigate the impact of QSM fiber on coherent optical system performance, we plot PIF contours based on (23) for the ideal case when there is no MPI at the output of the receiver, e.g., due to perfect electronic MPI compensation (see Fig. 9). For the PIF calculation, we

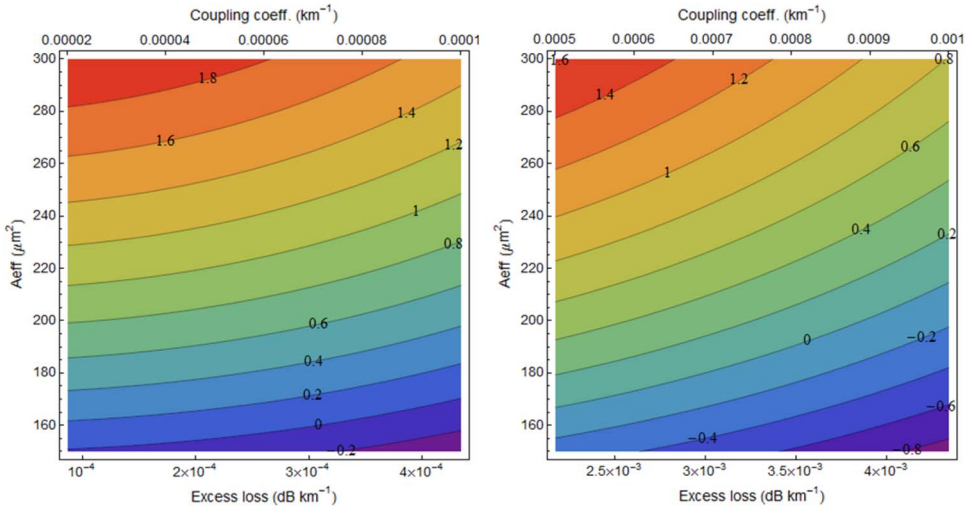

Fig. 10. PIF contours (in dB) as a function of the excess loss or the coupling coefficient and the effective area for a coherent optical communications system with 100-km spans and no electronic MPI compensation at the receiver. (a) Low DMA ($\Delta\alpha = 2 \times 10^{-3}$ dB/km). (b) High DMA ($\Delta\alpha = 4$ dB/km).

assume $n_2 = 2.1 \times 10^{-20}$ m^2/W at $\lambda = 1550$ nm, number of WDM channels $N_{ch} = 8$, symbol rate $R_s = 32$ GBd, amplifier noise figure $F_A = 5$ dB, a matched filter receiver with equivalent optical bandwidth equal to the symbol rate R_s, and $\Delta\nu = 12.5$ GHz. As a reference fiber we use a commercially available, large effective area submarine single-mode fiber with $\alpha_r = 0.155$ dB/km, $A_{eff,r} = 150$ μm^2, and dispersion $\beta_{2r} = 20.6$ ps/nm/km. We assume that the QSM fiber has the same fiber parameters as the reference fiber, except for the effective area and the excess loss. To calculate the latter, the coupling coefficient is varied in the range $[5 \times 10^{-4}, 5 \times 10^{-3}]$ km^{-1}. From Fig. 9, we observe that a hypothetical QSM fiber with 250 μm^2 effective area can provide 1 dB performance advantage over the reference fiber, if the coupling coefficient is at most $\kappa = 0.002$ km^{-1} for 100-km spans and $\kappa = 0.0045$ km^{-1} for 50-km spans.

Next, we plot PIF contours based on expression (29) for the case when there is no electronic MPI compensation (Fig. 10 for a system with 100-km spans of QSM fiber and Fig. 11 for a system with 50-km spans of QSM fiber). The same reference fiber is assumed, with $\alpha_r = 0.155$ dB/km and $A_{eff,r} = 150$ μm^2. Now, we assume that the QSM fiber differs from the reference fiber in the effective area, the excess loss, and the DMA. We distinguish two cases of DMA, a low value [see Figs. 10(a) and 11(a)] and a high value [see Figs. 10(b) and 11(b)]. For instance, from Fig. 10(b), we observe that for an effective area of 250 μm^2 and 100 km spans, the maximum allowable coupling coefficient is $\kappa_{max} = 6 \times 10^{-4}$ km^{-1} for $\Delta\alpha = 4$ dB/km to achieve QSM fiber PIF $= 1$ dB. We also observe that for an effective area of 250 μm^2 and 50 km spans, the maximum allowable coupling coefficient is $\kappa_{max} = 5 \times 10^4$ km^{-1} for $\Delta\alpha = 4$ dB/km to achieve QSM fiber PIF $= 1$ dB.

Finally, in Fig. 12(a), we plot graphs of the maximum allowable coupling coefficient as a function of the effective area and different span lengths for a coherent optical communications system with perfect electronic MPI compensation. (The maximum allowable coupling coefficient is the one to achieve PIF $= 1$ dB.) In Fig. 12(b), we plot graphs of the maximum allowable coupling coefficient as a function of the DMA for different values of the effective area for a coherent optical communications system with no MPI compensation and either 100-km spans (solid lines) or 50-km spans (broken lines). We observe that the lines for the 50-km spans cross with the lines of the 100-km spans in Fig. 12(b). It is worth noting that, for $A_{eff,r} \leq 210$ μm^2, it is impossible for QSM fiber to yield a 1 dB PIF compared to the single-mode reference fiber, even if the coupling

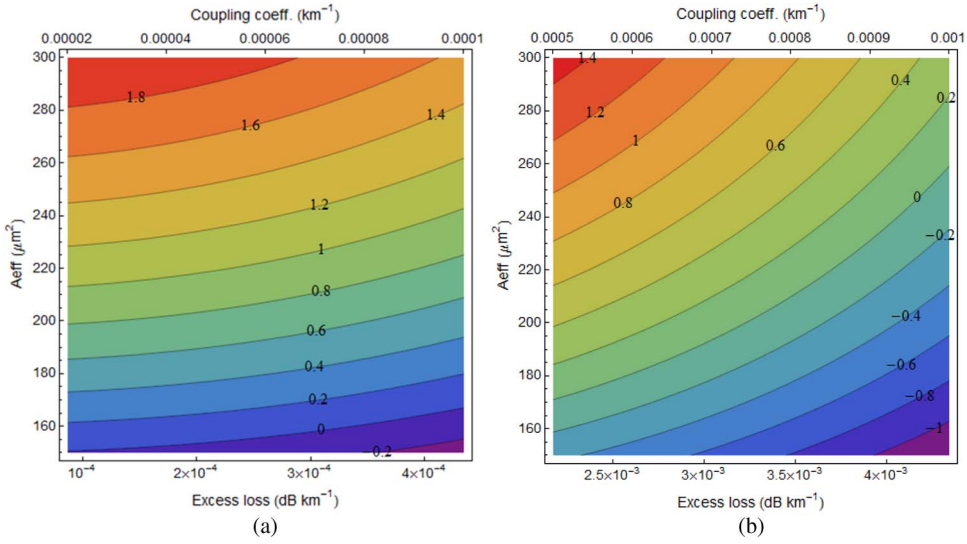

Fig. 11. PIF contours (in dB) as a function of the excess loss or the coupling coefficient and the effective area for a coherent optical communications system with 50-km spans and no electronic MPI compensation at the receiver. (a) Low DMA ($\Delta\alpha = 2 \times 10^{-3}$ dB/km). (b) High DMA ($\Delta\alpha = 4$ dB/km).

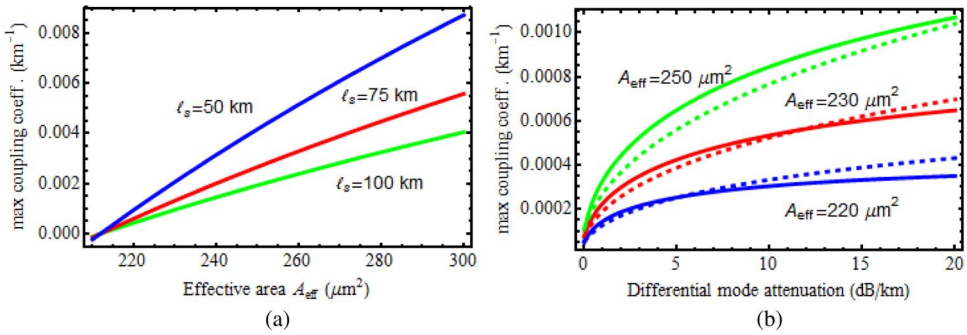

Fig. 12. Maximum allowable coefficient to achieve PIF = 1 dB. (a) In the case of perfect electronic MPI compensation at the receiver. (b) In the case of no electronic MPI compensation at the receiver. Symbols: solid lines: 100 km spans; broken lines: 50 km spans.

coefficient is $\kappa = 0$. Therefore, in the above plots, we assume that the QSM fiber effective area can be up to 300 μm^2.

4. Summary

In summary, we derived analytical expressions that relate the MPI, the power coupling coefficient, the DMA, and the span length using a continuous two-mode power CMT model. In the regime of interest, such expressions can provide examples of the interplay among these parameters, as shown in Figs. 4–6. We showed, for the first time, that the effect of MPI in a fiber can be reduced by the increase of DMA, and discussed the notion of the excess loss. We also pointed out possible errors in the results obtained by a discrete MPI approximation to continuous MPI and the compatibility of results of a segmented field CMT model with the power CMT description.

Furthermore, we introduced the PIF as the square of the ratio of the optimal Q-factor for the fiber under study and the optimal Q-factor of a reference fiber. We used this measure to derive

analytical expressions for the performance improvement of long-haul coherent optical communications systems using QSM fibers, where we took into account the impact of excess loss and MPI on system performance. From these expressions, we can calculate the maximum allowable coupling coefficient for different values of the DMA. We showed, for example, that a QSM fiber with an effective area of 250 μm^2, coupling coefficient $\kappa \leq 6 \times 10^{-4}$ km^{-1}, for $\Delta\alpha = 4$ dB/km offers 1 dB performance advantage over a reference pure silica single-mode fiber for 100 km spans when MPI is uncompensated. For fully compensated MPI, and thus arbitrary DMA, the maximal coupling coefficient should be smaller than 0.002 km^{-1} for 100 km spans, which is a value approximately 3.3-times larger than the maximal coupling coefficient required in the corresponding uncompensated MPI case.

Acknowledgment

The authors would like to thank W. A. Wood, D. Pikula, J. Hurley, A. Korolev, and V. Nazarov of Corning Incorporated for useful discussions.

Appendix

In this Appendix, we combine the formalism of [3], [13]–[16] in order to quantify the impact of MPI on the performance of coherent optical systems using single-mode transmission over quasi-single mode, few-mode and multimode fibers. The fundamental assumption behind our model is that MPI can be well represented as an additive white Gaussian noise at the sampling instant at the output of the coherent optical receiver.

In coherent optical systems with polarization division multiplexed (PDM) M-ary quadrature amplitude modulation (M-QAM) in the presence of Gaussian noise, the bit error probability is given by

$$P_{e|b} = \frac{1}{2}\mathrm{erfc}\left(\frac{Q}{\sqrt{2}}\right) \tag{A1}$$

where

$$\mathrm{erfc}(x) = \frac{2}{\sqrt{\pi}}\int_x^\infty e^{-t^2}dt.$$

The square of the Q-factor is asymptotically proportional to the optical signal-to-noise ratio (OSNR) at the receiver input [1]

$$Q^2 = \frac{3}{M-1}\frac{\Delta\nu}{B_{eq}}\mathrm{OSNR} \tag{A2}$$

where $\Delta\nu$ is the resolution bandwidth for the measurement of the OSNR, B_{eq} is the equivalent noise bandwidth of the coherent optical receiver, and M is the number of symbols in the QAM alphabet.

Assume that MPI generates an additive white Gaussian noise at the sampling instant with zero mean and variance σ_x^2, as measured at the equivalent noise bandwidth of the coherent optical receiver. Then, the OSNR in (A2) can be replaced by an effective OSNR, which is denoted by $\mathrm{OSNR}_{\mathrm{eff}}$ [13]–[16]:

$$\mathrm{OSNR}_{eff} = \frac{P}{\widetilde{\alpha} + \sigma_{x,eq}^2 + \widetilde{\gamma}P^3} \tag{A3}$$

where P is the total average launch power per channel (in both polarizations), and $\sigma_{x,eq}^2$ is the variance of a fictitious additive white Gaussian noise at the entrance of the coherent optical

receiver, measured at the resolution bandwidth $\Delta\nu$, that gives rise to the MPI generated noise at the sampling instant. Since we assumed a white crosstalk noise spectrum, we can write

$$\sigma^2_{x,eq} = \frac{\Delta\nu}{B_{eq}}\sigma^2_x. \tag{A4}$$

We calculate MPI at the entrance of the decision device at the coherent optical receiver as

$$MPI = \frac{\sigma^2_x}{P}. \tag{A5}$$

Next, we calculate the MPI from its definition (A5) for a coherent optical system, where the signal and N interferers arrive with aligned states of polarization [14]. The transmitted signal in one state of polarization is

$$E_s = \sum_m c_m g(t - mT) e^{i\phi(t)} \tag{A6}$$

where c_m are the QAM symbols, T is the symbol period, $g(t)$ the pulse shape (e.g., $g(t) = 1$ if $|t| \leq T/2$), and $\phi(t)$ the phase noise of the transmitter laser. We assume that the actual signal at the decision device of the receiver after ideal digital signal processing (DSP) equalization, in the absence of noise and residual distortion, can be written in continuous time t as

$$E_r(t) = E_s(t) + \sum_{k=1}^{N} \sqrt{\varepsilon_k} E_s(t - \tau_k) e^{-i\theta_k} \tag{A7}$$

where $\varepsilon_k = P_k/P$ are the crosstalk levels, τ_k are the group delays of the interferers, and θ_k are random phases accumulated along the various optical paths.

We assume that the group delays of the interferers are equal to multiples of the symbol period. This is the worst-case scenario of alignment according to [16]. Then, the (phase-rotated) signal detected after ideal DSP equalization at the sampling instant t_n is

$$E_r(t_n) = c_n + \sum_{k=1}^{N} \sqrt{\varepsilon_k} c_{n-k} e^{-i[\phi(t_n) - \phi(t_n - \tau_k)]} e^{-i\theta_k}. \tag{A8}$$

The interferometric noise due to crosstalk is then

$$n_x(t_n) = \sum_{k=1}^{N} \sqrt{\varepsilon_k} c_{n-k} e^{-i[\phi(t_n) - \phi(t_n - \tau_k)]} e^{-i\theta_k}. \tag{A9}$$

Taking the ensemble average of (A9) yields

$$\begin{aligned} \mu_x \equiv & \mathrm{E}\{n_x(t_n)\} \\ = & \sum_{k=1}^{N} \sqrt{\varepsilon_k}\, \mathrm{E}\{c_{n-k}\} \mathrm{E}\left\{e^{-i[\phi(t_n) - \phi(t_n - \tau_k)]}\right\} \mathrm{E}\{e^{-i\theta_k}\}. \end{aligned} \tag{A10}$$

The mean is zero because the constellation is symmetric in the complex plane and centered around the origin; therefore, $\mathrm{E}\{c_{n-k}\} = 0$. The variance of the crosstalk noise is

$$\sigma^2_x \equiv \mathrm{E}\left\{|n_x(t_n)|^2\right\} = \sum_{k=1}^{N} \varepsilon_k \mathrm{E}\left\{|c_{n-k}|^2\right\} = \mathrm{E}\left\{|c_n|^2\right\} \sum_{k=1}^{N} \varepsilon_k. \tag{A11}$$

The launched average power of the signal is the variance of the signal in the absence of crosstalk

$$P = \sigma_s^2 = \mathrm{E}\left\{|c_n|^2\right\}. \tag{A12}$$

By substituting (A11), (A12) into (A5), we obtain

$$MPI = \frac{\sigma_x^2}{P} = \sum_{k=1}^{N} \varepsilon_k \tag{A13}$$

which agrees with the original definition of MPI given in Section 2.

From (A4) and (A13), we conclude that the $\widetilde{\beta}$ coefficient in (27) is, for a matched filter receiver $(B_{\mathrm{eq}} = R_{\mathrm{s}})$, in the case of N_{s} spans, when mode stripping occurs between spans, $\widetilde{\beta} = N_{\mathrm{s}}\Delta\nu\, MPI/R_{\mathrm{s}}$, indeed.

References

[1] R.-J. Essiambre, G. Kramer, J. Winzer, J. Foschini, and B. Goebel, "Capacity limits of optical fiber networks," *J. Lightw. Technol.*, vol. 28, no. 4, pp. 662–701, Feb. 2010.

[2] S. Ramachandran, J. W. Nicholson, S. Ghalmi, and M. F. Yan, "Measurement of multipath interference in the coherent crosstalk regime," *IEEE Photon. Technol. Lett.*, vol. 15, no. 8, pp. 1171–1173, Aug. 2003.

[3] W. Zheng *et al.*, "Measurement and system impact of multipath interference from dispersion compensating fiber modules," *IEEE Trans. Instrum. Meas.*, vol. 53, no. 1, pp. 15–23, Feb. 2004.

[4] F. Yaman, N. Bai, B. Zhu, T. Wang, and G. Li, "Long distance transmission in few-mode fibers," *Opt. Exp.*, vol. 18, no. 12, pp. 13250–13257, Jun. 2010.

[5] F. Yaman *et al.*, "10 × 112Gb/s PDM-QPSK transmission over 5032 km in few-mode fibers," *Opt. Exp.*, vol. 18, no. 20, pp. 21342–21349, Sep. 2010.

[6] J. D. Downie *et al.*, "Transmission of 112 Gb/s PM-QPSK signals over up to 635 km of multimode optical fiber," *Opt. Exp.*, vol. 19, no. 26, pp. B363–B369, Dec. 2011.

[7] F. Yaman, E. Mateo, and T. Wang, "Impact of modal crosstalk and multi-path interference on few-mode fiber transmission," in *Proc. OFC*, Los Angeles, CA, USA, 2012, pp. B1–3, Paper OTu1D.2.

[8] N. A. Kaliteevskiy, A. E. Korolev, K. S. Koreshkov, V. N. Nazarov, and P. M. Sterlingov, "Two-mode coupling model in a few mode fiber," *Opt. Spectroscopy*, vol. 114, no. 6, pp. 913–916, Jun. 2013.

[9] N. Bai, C. Xia, and G. Li, "Adaptive frequency-domain equalization for the transmission of the fundamental mode in a few-mode fiber," *Opt. Exp.*, vol. 20, no. 21, pp. 24010–24017, Oct. 2012.

[10] S. Qi *et al.*, "256 Gb/s PM-16-QAM quasi-single-mode transmission over 2600 km using few-mode fiber with multipath interference compensation," in *Proc. OFC*, San Francisco, CA, USA, 2014, pp. 1–3, Paper M3C.5.

[11] Q. Sui *et al.*, "Long-haul quasi-single-mode transmissions using few-mode fiber in presence of multi-path interference," *Opt. Exp.*, accepted for publication.

[12] D. Marcuse, "Coupled power theory," in *Theory of Dielectric Optical Waveguides,* 2nd ed. New York, NY, USA: Academic, 1991, pp. 177–250.

[13] P. Poggiolini, A. Carena, V. Curri, G. Bosco, and F. Forghieri, "Analytical modeling of non-linear propagation in uncompensated optical transmission links," *IEEE Photon. Technol. Lett.*, vol. 23, no. 11, pp. 742–744, Jun. 2011.

[14] P. Poggiolini, "The GN model of non-linear propagation in uncompensated coherent optical systems," *J. Lightw. Technol.*, vol. 30, no. 24, pp. 3857–3879, Dec.15, 2012.

[15] A. Carena, V. Curri, G. Bosco, P. Poggiolini, and F. Forghieri, "Modeling of the impact of nonlinear propagation effects in uncompensated optical coherent transmission links," *J. Lightw. Technol.*, vol. 30, no. 10, pp. 1524–1539, May 2012.

[16] K.-P. Ho, "Effects of homodyne crosstalk on dual-polarization QPSK signals," *J. Lightw. Technol.*, vol. 29, no. 1, pp. 124–131, Jan. 2011.

[17] J. D. Downie, J. Hurley, I. Roudas, K. Koreshkov, and M. Mlejnek, *Multi-Path Interference Characterization in Few-Mode Fibers for Quasi-Single Mode Transmission*, unpublished.